Many-body perturbation theory for spin-forbidden two-photon spectroscopy of *f*-element compounds and its application to Eu^{2+} in CaF_2

C. K. Duan* and M. F. Reid
Department of Physics and Astronomy, University of Canterbury, Christchurch, New Zealand

G. W. Burdick
Department of Physics, Andrews University, Berrien Springs, Michigan 49104
(Received 25 March 2002; published 23 October 2002)

Predictions of the two-photon transition intensities for Eu^{2+} in CaF_2 generally give poor agreement with experiment because the low-lying excited states make a straightforward application of perturbation theory unreliable. In this work we explicitly include the effective Coulomb interaction and the crystal-field interaction for the excited configuration in the zeroth-order Hamiltonian, and treat the spin-orbit interaction as a perturbation. We obtain a good agreement with measured multiplet to multiplet two-photon absorption intensities. The linewidths of the two-photon absorption peaks, which vary dramatically, are explained by selection rules for nonradiative relaxation.

DOI: 10.1103/PhysRevB.66.155108 PACS number(s): 78.40.−q, 78.20.−e, 78.55.Hx, 33.50.−j

I. INTRODUCTION

Two-photon laser spectroscopy has been an important complementary technique to linear spectroscopy of solids, as it has a different parity selection rule, allows access to higher energy states, and has a greater variety of possible polarizations than linear spectroscopy.[1] Extensive measurements of two-photon absorption (TPA) intensities in rare-earth compounds by Dagenais *et al.*[2] and Downer and co-workers[3–6] could not be explained by the early lowest-order theory developed by Axe[7] in 1964: the angular-momentum selection rule $\Delta J \leqslant 2$ predicted by Axe's theory was completely violated as there are intense transitions with ΔL and ΔJ as large as six, and line strengths and polarization anisotropies were not correctly calculated. There are many theoretical developments that address this puzzle, which will be described in more detail below. These methods account for most of the discrepancies between the predictions of Axe's theory and measurements for Gd^{3+} in LaF_3,[4] but poorly predict the relative intensities for Eu^{2+} in CaF_2.[6] These discrepancies are sometimes referred to as ''the weakness of the third-order spin-orbit contributions.''[1] In addition to the intensity anomalies, the drastic variations of linewidths of TPA peaks are also puzzling.

The starting point of TPA theory is usually the second-order term of time-dependent perturbation theory. This term involves a summation over all possible intermediate states of the product of two one-photon transition matrix elements weighted by an energy denominator. The states involved are exact eigenstates of the full static Hamiltonian for the system when time-dependent perturbations are turned off. Usually approximations of the full static Hamiltonian and truncation to the summation are necessary. Time-independent perturbation theory is often adopted.[8] Axe's theory is zeroth order in time-independent perturbation theory in the sense that the splitting within f^N or the intermediate configurations is not considered. For the TPA to $^6P_{7/2}$, $^6P_{5/2}$ and $^6P_{3/2}$ of Gd^{3+} in LaF_3 using a single linearly polarized beam,[2] Axe's theory predicted 69:29:1, in contrast to the measured ratio 320:5.4:1. Judd and Pooler introduced a first-order spin-orbit perturbation to the intermediate states and predicted an intensity ratio 470:3.4:1,[9] which is close to the measured ratio. In addition, their calculations also accounted for the polarization dependence of the TPA measured by Downer and Bivas.[4] Downer and Bivas's measurements also showed the complete violation of orbit and total angular-momentum selection rules, which are explained by extending Judd-Pooler approach to include perturbations due to the effect of the crystal-field interaction on $5d$ orbitals in the intermediate states. Note that the ''third-order'' and ''fourth-order'' in many theoretical work on two-photon transitions[1,4,5,10,11] are ''first order'' and ''second order'' here, respectively in the sense of time-independent perturbation. The general expressions of the Judd-Pooler-Downer theory (often referred to as JPD theory in the literature) for orbit- and spin-forbidden transition were given by Ceulemans and Vandenberghe.[10] Calculations have been carried out for Tb^{3+} in a cubic lattice,[11] Sm^{2+} in SrF_2,[12,13] Eu^{2+} in CaF_2 and SrF_2 (Ref. 6) and $KMgF_3$,[14] and Cm^{3+}[15] and Eu^{3+}[16] in $LuPO_4$, in addition to Gd^{3+} in LaF_3. However, application of JPD theory to Eu^{2+} in CaF_2 is less successful.[6] The predicted intensity ratios for the linearly polarized transitions $^8S_{7/2} \rightarrow {}^6P_{7/2}$ and $^6D_{7/2}$ relative to $^6D_{9/2}$ are larger than the measured ratios by factors of more than 100 and 10 times, respectively. This has been referred to as ''the weakness of the third-order spin-orbit contributions.''[1] For transitions to the ^6I multiplets the calculated intensities are 5–10 times smaller than the measured intensities. Downer *et al.* reasoned that a significant part of the discrepancy results from a breakdown of closure approximation, i.e., the approximation that the $4f^6 5d$ configuration is degenerate. For the Eu^{2+} ion in CaF_2 and SrF_2, the lowest energy levels of the $4f^6 5d$ configuration are only about 25 000 cm^{-1} above the $^8S_{7/2}$ ground state of the $4f^7$ configuration, and in fact are below the ^6P levels of $4f^7$. However, Downer *et al.* were unable to improve their calculation significantly by relaxing the closure approximation. With a reasonable choice of spin-orbital interaction strength,

the ${}^8S_{7/2} \rightarrow {}^6P_{7/2}$ absorption rates for the circularly polarized beam and the ${}^8S_{7/2} \rightarrow {}^6P_{5/2}$ absorption rates are greatly reduced, but the linearly polarized absorption of ${}^6P_{7/2}$ decreases by only a factor of 4–5. Therefore, this does not solve the ''the weakness of the third-order spin-orbit contributions,'' and even makes the relative strength between linearly and circularly polarized transitions to ${}^7P_{7/2}$ worse. Such a situation also occurs in Eu^{2+}-doped $KMgF_3$, where the crystal-field interactions are much weaker, showing that the puzzle is not closely related to the strength of the crystal field.

There are some other attempts to simulate the TPA intensities in rare-earth ions. Burdick and Reid applied many-body perturbation theory (MBPT) techniques to develop a consistent approach to include various perturbations.[17] These calculations are roughly equivalent to the Judd-Pooler calculations if both the spin-orbit interaction and Coulomb interaction are included to infinite order.[18] The Burdick-Reid approach fails to converge for Eu^{2+} in CaF_2 because the Coulomb interaction is larger than the energy denominators for the low-lying $4f^6 5d$ excited configuration. Instead of using perturbation theory, Burdick *et al.*[19] did a calculation of the TPA of Eu^{2+}:CaF_2 by explicitly summing over all the intermediate free ion states of $4f^6 5d$. This gave good agreement with measurements for ${}^6P$ and ${}^6D$ levels, but the intensities for the TPA to ${}^6I$ states are forbidden by orbital angular-momentum selection rules under such an approximation.

It is now possible to explicitly calculate the energy levels of the $4f^6 5d$ excited states, including the Coulomb interaction, spin-orbit interaction and crystal-field interaction.[20] We are carrying out a detailed TPA calculation for Eu^{2+} in CaF_2 by summing over all of these states.[21] However, with such a complex and time-consuming calculation, the results are difficult to interpret and the effect of changes to the parameters are difficult to determine. Furthermore, including more intermediate states such as $4f^6 ng$ would greatly increase the computational time, and so this is impractical.

Besides the puzzle of the TPA intensities, the variation of the TPA linewidth and the mechanism of relaxation are also puzzling for Eu^{2+} in CaF_2: Some absorption lines of the ${}^6I$ energy levels are much narrower than other lines, and the absorption line of ${}^6D_{1/2}$ is almost an order of magnitude narrower than other neighboring ${}^6D$ lines.

In this paper we show that it is possible to explain the TPA intensities with a relatively simple perturbation calculation, similar to the JPD theory. We do this by a careful choice of the zero-order Hamiltonian. The strongest interactions, the $5d$ crystal-field interaction and the part of the Coulomb interaction that splits states with different spins, are included in the zero-order Hamiltonian. The spin-orbit interaction is treated as a perturbation. The special properties of the half-filled $4f^7$ shell are also exploited to simplify the calculation. We present the method using many-body perturbation theory and group theory, with details for the case of an ion site with O_h symmetry. The application to Eu^{2+} in CaF_2 predicts relative multiplet to multiplet transition intensities comparable to observations, and demonstrates the dependence of the intensities on ξ_{5d}/ξ_{4f}. The TPA linewidths of Eu^{2+}:CaF_2 are also analyzed qualitatively by exploring the selection rules for the nonradiative relaxation of the $4f^7$ states to $4f^6 5d$ states.

II. EFFECTIVE TWO-PHOTON TRANSITION OPERATORS SUITABLE FOR ORBIT- OR SPIN-FORBIDDEN TRANSITIONS

For ions with a half-filled, or nearly half-filled, f shell, there is a large gap between the ground multiplets (${}^8S_{7/2}$ for f^7 and ${}^7F_{0\text{-}6}$ for f^6 and f^8) of maximum spin and the excited states of reduced spin. The measured TPA is between energy levels of the ground multiplet and energy levels of the excited multiplets with spin of one electron flipped. The two-photon transitions are parity allowed because there are two odd-parity electric-dipole operators involved, connecting the initial and final states to intermediate states of opposite parity. These opposite-parity states may include d and g-electron excited states, d-electron core excitations, and continuum d and g states, as well as ligand states with d- and g-electron character. However, as the $nf^{N-1}(n+1)d$ states have the lowest energies, they may be expected to dominate. The transitions are spin forbidden, so that the mixing of states by the spin-orbit interaction plays an essential role. Some of the transitions are also orbit forbidden ($\Delta L > 2$) and therefore the crystal-field interactions, especially the strong d-electron crystal-field interaction, are also important. The Coulomb interaction does not provide any relaxation of the spin- or orbit-forbidden selection rules, and therefore was not included in the JPD theory.[22] However, the splitting caused by the Coulomb interaction will significantly affect the calculation due to a modification of the energy denominator (i.e., it causes a breakdown of the closure approximation) and thus must also be considered. For the trivalent ions, the Coulomb interaction may be treated as a perturbation, but for the divalent ions we wish to consider here, the usual perturbation expansion will diverge. The perturbation expansion of the d-electron crystal-field interactions converges slowly because the magnitudes of those interactions are comparable to the nf-$(n+1)d$ splitting.

In contrast to previous work, for the calculations considered below we include the most important parts of the Coulomb interaction, i.e., the spin-flip energy for f and d electrons, and the d-electron crystal-field interaction into the zeroth-order Hamiltonian:

$$H_0 = \sum_i \epsilon_i a_i^\dagger a_i . \tag{1}$$

Here $a^\dagger$ and a are creation and annihilation operators, respectively, and ϵ_i is the one-particle energy for energy level i.

A schematic diagram of the ''one-particle'' energy levels in a cubic site is shown in Fig. 1. Notice that the spin directions indicated are only in the sense of parallel and antiparallel to the total spin of the maximum-spin states, and have nothing to do with the particular frame chosen. In the particular case here, the lowest $4f^6 5d$ level is lower than the sextet states of $4f^7$ due to crystal-field splitting, which is reflected by $e_\uparrow$ being lower than $4f_\downarrow$. The other interactions

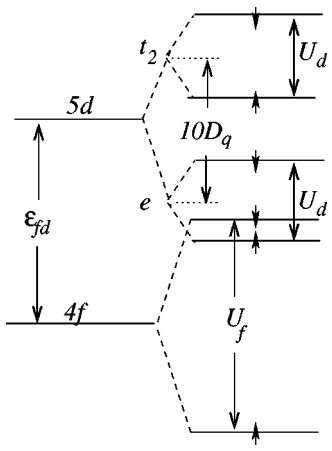

FIG. 1. Schematic diagram for one-particle energy levels in a cubic site. ϵ_{fd} is the difference between the average energy of the nf orbitals and the $(n+1)d$ orbitals. U_f and U_d are the exchange splittings for f and d orbitals, respectively, which are assumed to be isotropic. $10D_q$ is the splitting of $(n+1)d$ orbitals in a cubic site. The spin-orbit splitting and the crystal-field splitting for nf are neglected.

not included in H_0, the spin-orbit interactions $V_{\rm so}(ff)$ and $V_{\rm so}(dd)$, the crystal-field interactions $V_c(ff)$, and the remaining Coulomb interactions $V'_{\rm Coul}$, are considered as perturbations, i.e.,

$$V=V_{\rm so}(ff)+V_{\rm so}(dd)+V_c(ff)+V'_{\rm Coul}. \tag{2}$$

For Eu^{2+} the $4f^7$ ground states can be written as $4f^7_\uparrow$ and the ground-state model space is chosen to contain only this set of states. The excited states of interest for the TPA are written as $4f^5_\uparrow(4f_\uparrow 4f_\downarrow)$ and the excited-state model space is chosen to contain only these states. For ions with f^6 and f^8 ground configurations, the ground and excited states may be written as $f^6_\uparrow$, $f^6_\uparrow(f_\uparrow f_\downarrow)$ and $f^4_\uparrow(f_\uparrow f_\downarrow)$, $f^4_\uparrow(f_\uparrow f_\downarrow)^2$, respectively.

According to MBPT, an effective operator $T_{\rm TPA}$ that acts between the ground-state model space and the excited-state model space eigenvectors to give the exact transition matrix elements can be constructed, provided that the model space eigenvectors are appropriately normalized projections of the exact eigenvectors. The effective operator is usually expanded order by order in the perturbation V, and is represented by diagrams. The matrix element of $T_{\rm TPA}$ between a basis function $|I\rangle_0$ in the ground-state model space and a basis function $|F\rangle_0$ in the excited-state model space can be calculated from those diagrams. Since the two model-space bases have well-defined spins and the electric dipole moment operator does not change the spin, the zeroth-order term of $T_{\rm TPA}$ is zero. In first order, only

$$V_{\rm so}=V_{\rm so}(ff)+V_{\rm so}(dd) \tag{3}$$

contributes. Three first-order terms have nonzero contributions:

$$\sum_{S,Q_I}\frac{{}_0\langle F|\mathbf{D}\cdot\mathbf{e}|S\rangle_0\ {}_0\langle S|\mathbf{D}\cdot\mathbf{e}|Q_I\rangle_0\ {}_0\langle Q_I|V_{\rm so}|I\rangle_0}{[(E^0_I+E^0_F)/2-E^0_S](E^0_I-E^0_{Q_I})} \tag{4}$$

$$+\sum_{S_2,S_1}\frac{{}_0\langle F|\mathbf{D}\cdot\mathbf{e}|S_2\rangle_0\ {}_0\langle S_2|V_{\rm so}|S_1\rangle_0\ {}_0\langle S_1|\mathbf{D}\cdot\mathbf{e}|I\rangle_0}{[(E^0_I+E^0_F)/2-E^0_{S_2}][(E^0_I+E^0_F)/2-E^0_{S_1}]} \tag{5}$$

$$+\sum_{Q_F,S}\frac{{}_0\langle F|V_{\rm so}|Q_F\rangle_0\ {}_0\langle Q_F|\mathbf{D}\cdot\mathbf{e}|S\rangle_0\ {}_0\langle S|\mathbf{D}\cdot\mathbf{e}|I\rangle_0}{(E^0_F-E^0_{Q_F})[(E^0_I+E^0_F)/2-E^0_S]}. \tag{6}$$

In the expression, $|S\rangle_0$, $|S_1\rangle_0$, and $|S_2\rangle_0$ are eigenvectors of H_0, which are limited to the $f^{N-1}d$ and $f^{N-1}g$ configurations due to the parity and angular-momentum selection rules of the electric dipole operator $\mathbf{D}\cdot\mathbf{e}$. $|Q\rangle_I$ ($|Q\rangle_F$) must be in the spaces orthogonal to the ground-state model space and the excited-state model space, respectively. In the particular cases considered here, $|Q\rangle_I$ is in the excited-state model space and $|Q\rangle_F$ is in the ground-state model space. E^0 are the eigenvalues of H_0 for the corresponding bases denoted by the subscripts.

There are two nonzero diagrams for each of the three terms, which are shown in Fig. 2. MBPT tells us that the Pauli exclusion principle can be relaxed if it is done consistently, and the three disconnected diagrams cancel under this

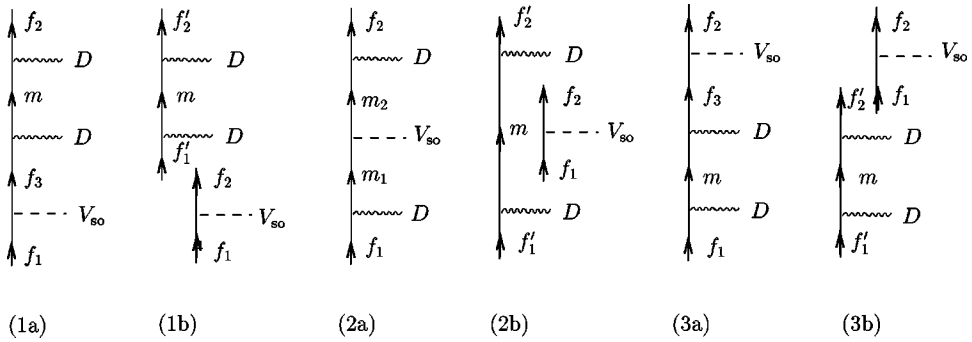

FIG. 2. First-order diagrams for two-photon transitions. f_1, f_2, f_3, f'_1, f'_2, and f'_3 are f shell orbitals, and m, m_1 and m_2 are orbitals with even parity. f_1 and f_2 are always parallel and antiparallel, respectively, to the total spin $S_{\rm max}$ of the maximum spin states of the half-filled shell. f'_1 and f'_2 are both parallel or both antiparallel to $S_{\rm max}$. The spin directions of the other orbitals are uniquely determined in each diagram by the fact that the spin of the outgoing particles cannot be changed by D vertices and is changed by a $V_{\rm so}$ vertex. The one-particle energy depends on the spin direction of the orbital.

choice. The cancelation can easily be verified for the three disconnected diagrams: the matrix elements are the same and the three factors from the denominators add up to zero.

Group theory and tensor techniques are widely used in spectroscopy to clarify selection rules and to simplify calculations. Eigenstates and (transition) operators can be expanded in terms of basis states and basis operators that have well-defined transformation properties under symmetry operations. Basis states and operators are labeled by irreducible representations (irreps) of a group chain that characterize the system. We choose the group chain for the ion site as $O_3^s \times O_3^l \supset O_3^j \supset G \supset C_1$, where G is the site symmetry. We denote the partner for this group chain as $s \cdot l^{\pm} a \lambda b$, where s is an irrep of O_3^s (with positive parity), $l^{\pm}$ is an irrep of O_3^l whose parity is denoted as a supscript, and $a\lambda b$ are labels for the $O_3^j \supset G \supset C_1$ group chain, with λ being an irrep of G and a and b being multiplicity labels. In the following we will often abbreviate $a\lambda b$ to a single label c and describe the labels of states or operators as $s \cdot l^{\pm} c$. Parity supscripts will also be neglected in most cases unless this causes ambiguities. For example, bases for f (d) orbitals will be labeled as $|1/2 \cdot 3 c_f\rangle$ ($|1/2 \cdot 2 c_d\rangle$) and a component of dipole moment operator will be labeled as $D^{0 \cdot 1c}$. The labels of irreps and multiplicities for point groups in this paper will follow Butler's convention.[23]

$\mathbf{D} \cdot \mathbf{e}$ can be expanded in terms of the electric dipole operator components $D^{0.1c}$ as

$$\mathbf{D} \cdot \mathbf{e} = \sum_c D^{0 \cdot 1c} e_{0 \cdot 1c}. \tag{7}$$

In order to evaluate the three connected diagrams, we use the general relation

$$\sum_i \frac{|i\rangle\langle i|}{\epsilon - \epsilon_i} = \frac{1}{\epsilon - h}, \tag{8}$$

where $|i\rangle$ and ϵ_i are normalized eigenvectors and eigenvalues of an arbitrary Hamiltonian operator h respectively, and ϵ is an arbitrary constant.

The three connected diagrams can be evaluated with MBPT diagram rules. We notice that the denominators in Eqs. (4)–(6) are slightly different from those of the third-order terms in an effective Hamiltonian. We will give the expression only for diagrams (2a). For (2a), m_1 and m_2 can be either d or g orbitals, with spins parallel and antiparallel to the initial maximum spin states, respectively. Here we will limit them to $(n+1)d$ orbitals, which are the most important contributions to T_{TPA}. The energies for m_1 and m_2 are $\epsilon_{fd} - U_d/2 + \epsilon'_{m_1}$ and $\epsilon_{fd} + U_d/2 + \epsilon'_{m_2}$, respectively. Here ϵ'_m ($m = m_1$ or m_2) is the crystal-field energy determined by the crystal-field Hamiltonian h^d_{cf}, which are $-6D_q$ and $4D_q$ for e and t_2 one-particle energy levels, respectively, for Eu^{2+} in CaF_2. By using the denominator rules required by Eq. (5) and then using Eq. (8) to replace the summation over energy denominators, $\Sigma_m |m\rangle\langle m| / [-(\epsilon_{fd} \pm U_d/2) - \epsilon'_m]$, (2a) can be written as

$$\begin{aligned}(2a) = & \sum_{c_{f_1}, c_{d_1}, c_{d_2}, c_{d_3}, c_{d_4}, c_{f_2}} a^{\dagger}_{1/2 \cdot 3 c_{f_1}} a_{1/2 \cdot 3 c_{f_2}} \\ & \times \langle 1/2 \cdot 3 c_{f_1} | \mathbf{D} \cdot \mathbf{e} | 1/2 \cdot 2 c_{d_1} \rangle \\ & \times \left\langle 1/2 \cdot 2 c_{d_1} \left| \frac{1}{-(\epsilon_{fd} + U_d/2) - h^d_{\mathrm{cf}}} \right| 1/2 \cdot 2 c_{d_2} \right\rangle \\ & \times \langle 1/2 \cdot 2 c_{d_2} | V_{\mathrm{so}} | 1/2 \cdot 2 c_{d_3} \rangle \\ & \times \left\langle 1/2 \cdot 2 c_{d_3} \left| \frac{1}{-(\epsilon_{fd} - U_d/2) - h^d_{\mathrm{cf}}} \right| 1/2 \cdot 2 c_{d_4} \right\rangle \\ & \times \langle 1/2 \cdot 2 c_{d_4} | \mathbf{D} \cdot \mathbf{e} | 1/2 \cdot 3 c_{f_2} \rangle. \end{aligned} \tag{9}$$

In the above expressions, the intermediate one-particle orbitals can only be in $(n+1)d$ orbital space, and therefore the projection operator for this space, $\Sigma_{c_{d_i}} |1/2 \cdot 2 c_{d_i}\rangle\langle 1/2 \cdot 2 c_{d_i}|$, has been inserted wherever appropriate. The expressions for the other two connected diagrams (1a) and (3a) can be derived in a similar manner.

As both V_{so} and the denominators are invariant under transformations of the site symmetry group G, the effective operator T_{TPA} must transform the same way as the two dipole moments do under group G. We shall make use of this property, the double tensor $W^{1 \cdot K c_K}$ and the polarization factor $(\mathbf{ee})_{D c_D}$ defined below to simplify the calculation in the following. $W^{1 \cdot K c_K}$ can be written in terms of $2jm$'s $(\cdots)$ and vector coupling coefficients $\langle \cdots, \cdots | \cdots \rangle$ (Ref. 23) as

$$W^{1 \cdot K c_K} = -(a^{\dagger}_{1/2 \cdot 3} \tilde{a}_{1/2 \cdot 3})^{1 \cdot K c_K} \tag{10}$$

$$\begin{aligned} = & -\sum_{c_1, c_2} a^{\dagger}_{1/2 \cdot 3 c_1} a_{1/2 \cdot 3 c_2} (1/2 \cdot 3 \;\; c_2^*) \\ & \times \langle 1/2 \cdot 3 c_1, 1/2 \cdot 3 c_2^* | 1 \cdot K c_K \rangle. \end{aligned} \tag{11}$$

The polarization factor $(\mathbf{ee})_{D c_D}$ is defined as

$$(\mathbf{ee})_{D c_D} = \sum_{c_1, c_2} \langle D c_D | 1 c_1, 1 c_2 \rangle e_{1 c_1} e_{1 c_2}. \tag{12}$$

T_{TPA} can be written in terms of $W^{1 \cdot K c_K}$ and $(\mathbf{ee})_{D c_D}$ as

$$T_{\mathrm{TPA}} = \sum_{K a_K, D a_D, \lambda} w_{K a_K, D a_D, \lambda} \sum_b W^{1 \cdot K K a_K \lambda b} (\mathbf{ee})_{D a_D \lambda b}, \tag{13}$$

where the coefficient

$$w_{Ka_K,Da_D;\lambda}=\sum_{i=1}^{3} w^{i}_{Ka_K,Da_D,\lambda} \tag{14}$$

is the sum of the corresponding coefficients from the three connected diagrams. We shall also make use of the following expansion for denominators:

$$\frac{1}{\epsilon-h^{5d}_{\rm cf}}=\sum_{Ka} \alpha_{Ka}(\epsilon)U^{0\cdot KKa00}(5d,5d), \tag{15}$$

where α_{Ka} can be written by using $2jm(\cdots)$, $3jms$ $(\cdots,\cdots,\cdots)$ and the dimension of an irrep $|\lambda|$ as[23]

$$\alpha_{Ka}(\epsilon)=\sum_{\lambda,a_1,a_2}\left\langle 1/2\cdot 2a_1\lambda\left|\frac{1}{\epsilon-h^{5d}_{\rm cf}}\right|1/2\cdot 2a_2\lambda\right\rangle \times\frac{|K|}{|\lambda|^{1/2}}(1/2\cdot 2\ \ a_1\ \ \lambda) \times(1/2\cdot 2\ \ a_1^*\ \ \lambda^*,\ \ 0\cdot K^+\ \ a\ \ 0,\ \ 1/2\cdot 2\ \ a_2\ \ \lambda). \tag{16}$$

In the following we shall use the reduced matrix elements (RME's) $\langle \eta_f s_f\cdot l_f a_f\lambda_f||T^{S\cdot La\lambda}||\eta_i s_i\cdot l_i a_i\lambda_i\rangle_m$, which can be calculated from $\langle \eta_f s_f\cdot l_f||T^{S\cdot L}||\eta_i s_i\cdot l_i\rangle$ with the Wigner-Ekart theorem. Here m is the multiplicity of λ_f in the coupling of λ and λ_i. With Eq. (15) and some complex but straightforward recoupling manipulations, the three coefficients $w^{i}_{Ka_K,Da_D,\lambda}$ can be written as

$$\begin{aligned}
w^{1}_{Ka_K\lambda_K,Da_D}=&-\sum_{\Delta,a_{f_1},\cdots,a_{f_2},\lambda_{f_1},\cdots,\lambda_{f_2},s_1,\cdots,s_4}\alpha_{\Delta a_\Delta}(-\epsilon_{fd}-U_d/2)/(-U_f)\\
&\times\langle 1\cdot Ka_K\lambda_K|1/2\cdot 3a_{f_1}\lambda_{f_1},1/2\cdot 3a^*_{f_2}\lambda^*_{f_2}\rangle_{s_3}\langle Da_D\lambda_K|D_1a_{D_1}\lambda_{D_1},D_2a_{D_2}\lambda_{D_2}\rangle^*_{s_4}\\
&\times\langle\lambda_{D_1}(\lambda_{D_2}\lambda_{f_2})s_2\lambda_d;s_1\lambda_{f_1}|(\lambda_{D_1}\lambda_{D_2})s_4\lambda_K,\lambda_{f_2};s_3\lambda_{f_1}\rangle|\lambda_K|^{-1/2}\{\lambda_K\}\{\lambda_{f_1}\lambda^*_{f_2}\lambda_K\}_{s_3}\\
&\times(1/2\cdot 3\ \ a^*_{f_2}\ \ \lambda^*_{f_2})\langle 1/2\cdot 3\ \ a_{f_1}\ \ \lambda_{f_1}||D^{0\cdot 1\ \ a_{D_1}\ \ \lambda_{D_1}}||1/2\cdot 2\ \ a_{d_1}\ \ \lambda_d\rangle_{s_1}\\
&\times|1/2\cdot 2|^{-1/2}\langle 1/2\cdot 2\ \ a_{d_1}\ \ \lambda_d||U^{0\cdot\Delta\ \ a_\Delta\ \ 0}||1/2\cdot 2\ \ a_{d_2}\ \ \lambda_d\rangle\\
&\times|1/2\cdot 2|^{-1/2}\langle 1/2\cdot 2\ \ a_{d_2}\ \ \lambda_d||D^{0\cdot 1\ \ a_{D_2}\ \ \lambda_{D_2}}||1/2\cdot 3\ \ a_{f_3}\ \ \lambda_{f_2}\rangle_{s_2}\\
&\times|1/2\cdot 3|^{-1/2}\langle 1/2\cdot 3\ \ a_{f_3}\ \ \lambda_{f_2}||V^{1\cdot 1\ \ a_{V_{\rm so}}\ \ 0}_{\rm so}||1/2\cdot 3\ \ a_{f_2}\ \ \lambda_{f_2}\rangle,
\end{aligned} \tag{17}$$

$$\begin{aligned}
w^{2}_{Ka_K\lambda_K,Da_D}=&-\sum_{\Delta_1,\Delta_2,a_{f_1},\cdots,a_{f_2},\lambda_{f_1},\cdots,\lambda_{f_2}s_1,\cdots,s_4}\alpha_{\Delta_1a_{\Delta_1}}(-\epsilon_{fd}-U_d/2)\alpha_{\Delta_2a_{\Delta_2}}(-\epsilon_{fd}+U_d/2)\\
&\times\langle 1\cdot Ka_K\lambda_K|1/2\cdot 3a_{f_1}\lambda_{f_1},1/2\cdot 3a^*_{f_2}\lambda^*_{f_2}\rangle_{s_3}\langle Da_D\lambda_K|D_1a_{D_1}\lambda_{D_1},D_2a_{D_2}\lambda_{D_2}\rangle^*_{s_4}\\
&\times\langle\lambda_{D_1}(\lambda_{D_2}\lambda_{f_2})s_2\lambda_d;s_1\lambda_{f_1}|(\lambda_{D_1}\lambda_{D_2})s_4\lambda_K,\lambda_{f_2};s_3\lambda_{f_1}\rangle|\lambda_K|^{-1/2}\\
&\times\{\lambda_K\}\{\lambda_{f_1}\lambda^*_{f_2}\lambda_K\}_{s_3}(1/2\cdot 3\ \ a^*_{f_2}\ \ \lambda^*_{f_2})\langle 1/2\cdot 3\ \ a_{f_1}\ \ \lambda_{f_1}||D^{0\cdot 1\ \ a_{D_1}\ \ \lambda_{D_1}}||1/2\cdot 2\ \ a_{d_1}\ \ \lambda_d\rangle_{s_1}\\
&\times|1/2\cdot 2|^{-1/2}\langle 1/2\cdot 2\ \ a_{d_1}\ \ \lambda_d||U^{0\cdot\Delta_1\ \ a_{\Delta_1}\ \ 0}||1/2\cdot 2\ \ a_{d_2}\ \ \lambda_d\rangle|1/2\cdot 2|^{-1/2}\\
&\times\langle 1/2\cdot 2\ \ a_{d_2}\ \ \lambda_d||V^{1\cdot 1\ \ a_{V_{\rm so}}\ \ 0}_{\rm so}||1/2\cdot 2\ \ a_{d_3}\ \ \lambda_d\rangle|1/2\cdot 2|^{-1/2}\\
&\times\langle 1/2\cdot 2\ \ a_{d_3}\ \ \lambda_d||U^{0\cdot\Delta_2\ \ a_{\Delta_2}\ \ 0}||1/2\cdot 2\ \ a_{d_4}\ \ \lambda_d\rangle|1/2\cdot 2|^{-1/2}\\
&\times\langle 1/2\cdot 2\ \ a_{d_4}\ \ \lambda_d||D^{0\cdot 1\ \ a_{D_2}\ \ \lambda_{D_2}}||1/2\cdot 3\ \ a_{f_2}\ \ \lambda_{f_2}\rangle_{s2},
\end{aligned} \tag{18}$$

$$w^3_{Ka_K\lambda_K,Da_D} = -\sum_{\Delta,a_{f_1},\cdots,a_{f_2},\lambda_{f_1},\cdots,\lambda_{f_2}s_1,\cdots,s_4} \alpha_{\Delta a_\Delta}(-\epsilon_{fd}+U_d/2)/(U_f)$$
$$\times\langle 1\cdot Ka_K\lambda_K|1/2\cdot 3a_{f_1}\lambda_{f_1},1/2\cdot 3a^*_{f_2}\lambda^*_{f_2}\rangle_{s_3}\langle Da_D\lambda_K|D_1a_{D_1}\lambda_{D_1},D_2a_{D_2}\lambda_{D_2}\rangle^*_{s_4}$$
$$\times\langle\lambda_{D_1}(\lambda_{D_2}\lambda_{f_2})s_2\lambda_d;s_1\lambda_{f_1}|(\lambda_{D_1}\lambda_{D_2})s_4\lambda_K,\lambda_{f_2};s_3\lambda_{f_1}\rangle|\lambda_K|^{-1/2}$$
$$\times\{\lambda_K\}\{\lambda_{f_1}\lambda^*_{f_2}\lambda_K\}_{s_3}(1/2\cdot 3\ \ a^*_{f_2}\ \ \lambda^*_{f_2})\langle 1/2\cdot 3\ \ a_{f_1}\ \ \lambda_{f_1}||V^{1\cdot 1\ \ a_{V_{so}}\ \ 0}_{so}||1/2\cdot 3\ \ a_{f_3}\ \ \lambda_{f_1}\rangle|1/2\cdot 3|^{-1/2}$$
$$\times\langle 1/2\cdot 3\ \ a_{f_3}\ \ \lambda_{f_1}||D^{0\cdot 1\ \ a_{D_1}\ \ \lambda_{D_1}}||1/2\cdot 2\ \ a_{d_1}\ \ \lambda_d\rangle_{s_1}|1/2\cdot 2|^{-1/2}$$
$$\times\langle 1/2\cdot 2\ \ a_{d_1}\ \ \lambda_d||U^{0\cdot\Delta\ \ a_\Delta\ \ 0}||1/2\cdot 2\ \ a_{d_2}\ \ \lambda_d\rangle|1/2\cdot 2|^{-1/2}$$
$$\times\langle 1/2\cdot 2\ \ a_{d_2}\ \ \lambda_d||D^{0\cdot 1\ \ a_{D_2}\ \ \lambda_{D_2}}||1/2\cdot 3\ \ a_{f_2}\ \ \lambda_{f_2}\rangle_{s_2}. \tag{19}$$

In the above equations, the a's are branching multiplicities for $O^s_3\times O^l_3\supset G$, the λ's are irreps for group G, s's are coupling multiplicities for group G, $\langle\lambda_{D_1}(\lambda_{D_2}\lambda_{f_2})\cdots|(\lambda_{D_1}\lambda_{D_2})\cdots\rangle$ is a recoupling coefficient for irreps of G, $\{\lambda_K\}$ and $\{\lambda_{f_1}\lambda^*_{f_2}\lambda_K\}$ are $2j$ and $3j$ phases, and $|\lambda|$ is the dimension of irrep λ. All the factors determined solely by group theory are tabulated by Butler,[23] and can also be calculated with RACAH.[24]

The effective $T_{\rm TPA}$ operator can be used to calculate two-photon transition line strengths once the model-space eigenvectors are known. It is important to realize that our expressions for $T_{\rm TPA}$ are only valid when the bra and ket are in the excited- and ground-state model spaces, respectively, necessarily making the $T_{\rm TPA}$ operator not Hermitian. We denote the model space eigenvectors as $|\eta\lambda b\rangle$, where λ is the irrep for group G, b distinguishes the partners of λ, and η is a label to distinguish those states with the given symmetry labels (λ and b here). The line strength for the TPA $|\eta_f\lambda_f\rangle \leftarrow|\eta_i\lambda_i\rangle$ is

$$I(\eta_f\lambda_f,\eta_i\lambda_i)=\sum_{b_f,b_i}|\langle\eta_f\lambda_f b_f|T_{TPA}||\eta_i\lambda_i b_i\rangle|^2$$
$$=\sum_{D_1d_1D_2d_2\lambda}P_{D_1d_1,D_2d_2;\lambda}\times\frac{\langle\eta_f\lambda_f||T^\lambda_{D_1d_1}||\eta_i\lambda_i\rangle\langle\eta_f\lambda_f||T^\lambda_{D_2d_2}||\eta_i\lambda_i\rangle^*}{|\lambda|}, \tag{20}$$

where

$$P_{D_1d_1,D_2d_2;\lambda}=\sum_b(\mathbf{ee})_{D_1d_1\lambda b}(\mathbf{ee})^*_{D_2d_2\lambda b}, \tag{21}$$

$$T^\lambda_{Dd}=\sum_{SLJa}w_{S\cdot L\ Ja\ \lambda,\ Dd}W^{S\cdot L\ Ja\ \lambda}. \tag{22}$$

In this paper, we calculate only the total line strengths between two multiplets (η_iJ_i) to (η_fJ_f), where η are extra labels to distinguish multiplets with the same J label. This can be written as

$$I(\eta_fJ_f,\eta_iJ_i)=\sum_{D_1d_1D_2d_2Ja\lambda}P_{D_1d_1,D_2d_2;\lambda}\times\frac{\langle\eta_fJ_f||T^{Ja'\lambda}_{D1d_1}||\eta_iJ_i\rangle\langle\eta_fJ_f||T^{Ja'\lambda}_{D2d_2}||\eta_iJ_i\rangle^*}{2J+1}, \tag{23}$$

where

$$T^{Ja'\lambda}_{Dd}=\sum_{SL}w_{SLJa\lambda,Dd}W^{S\cdot LJ}, \tag{24}$$

and a' is the multiplicity for the branching $O^j_3\supset G$.

III. RELATIVE PROBABILITIES FOR MULTIPLET TO MULTIPLET TWO-PHOTON ABSORPTION OF Eu^{2+} IN CaF_2

In CaF_2 Eu^{2+} occupies Ca^{2+} site with O_h symmetry, with eight nearest F^-'s on the corners of a cube. The single-particle $4f$ and $5d$ energy levels are shown in Fig. 1. The TPA amplitude is calculated from Eq. (13), which requires various physical parameters as inputs. The average change in energies due to the exchange interaction when the spin of one of the $4f^7$ electrons is flipped is U_f, and when the spin of the $5d$ electron of $4f^65d$ is flipped is U_d. These may be calculated as

$$U_f=\frac{63}{8}E_1-\frac{200}{3}E_2=38\,000\ \ \mathrm{cm}^{-1}, \tag{25}$$

$$U_d=\frac{3}{5}G_1(4f,5d)+\frac{4}{15}G_3(4f,5d)+\frac{10}{33}G_5(4f,5d) \tag{26}$$

where E_1 and E_2 are Racah parameters, which are linear combination of $4f$-$4f$ Coulomb radial integrals $F_K(4f,4f)$

TABLE I. The polarization vectors and polarization factors for the three laser beams used in the measurements of Downer *et al.* (Ref. 6).

Label	Polarization vector	$P_{A_{1g}}$	P_{E_g}	$P_{T_{2g}}$
1 0 0	$\mathbf{z}$	1/3	2/3	0
1 1 1	$(\mathbf{x}+\mathbf{y}+\mathbf{z})/\sqrt{3}$	1/3	0	2/3
circular	$i(\mathbf{x}+\mathbf{y})/2\pm\mathbf{z}/\sqrt{2}$	0	3/8	5/8

$(K=2,4,6)$,[25] and $G_K(4f,5d)$ $(K=1,3,5)$ are $4f$-$5d$ Coulomb exchange radial integrals. The $F_K(4f,4f)$ values used here are the same as those used by Downer *et al.*[6] The $G_K(4f,5d)$ values can be determined from modified free-ion calculations.[26] The comparison of theoretical and experimental exchange splitting of $4f^{N-1}5d$ configuration for trivalent heavy lanthanides[20] indicates that the calculated values need to be scaled down roughly by a factor of 2/3, and this reduction is partly due to nephaluxic effects.[20] This would give $U_d \approx 7500\ \mathrm{cm}^{-1}$. The drastic broadening of TPA peaks can be better explained by a value of $U_d \approx 6500\ \mathrm{cm}^{-1}$ (see Sec. IV). So we shall use $U_d \approx 6500\ \mathrm{cm}^{-1}$ in our calculations. The crystal-field interaction splits the $5d$ orbitals into two energy levels, namely, e and t_2, by $10D_q$. From the one-photon spectra of Eu^{2+}:CaF_2 we obtain experimental values $\epsilon_{fd}=21\,000\ \mathrm{cm}^{-1}$ and $10D_q=16\,000\ \mathrm{cm}^{-1}$. The α coefficients of Eq. (16) are functions of these energy parameters. Only two of the α's are nonzero, i.e., α_0 which multiplies $U^{0\cdot 000}$ and α_4 which multiplies $U^{0\cdot 440}$. We obtain

$$\alpha_0(\epsilon)=\sqrt{\frac{2}{5}}\left(\frac{2}{\epsilon-\epsilon_{e_g}}+\frac{3}{\epsilon-\epsilon_{t_{2g}}}\right), \tag{27}$$

$$\alpha_4(\epsilon)=\frac{18}{\sqrt{15}}\left(\frac{1}{\epsilon-\epsilon_{e_g}}-\frac{1}{\epsilon-\epsilon_{t_{2g}}}\right), \tag{28}$$

where $\epsilon_{e_g}=-6D_q$ and $\epsilon_{t_{2g}}=4D_q$ are the one-particle energy levels (relative to the barycenter) of the $5d$ orbitals. The polarization dependence is greatly simplified for a site of O_h symmetry. There are only three polarization factors, which can be fully distinguished by the irreps $\lambda=A_{1g}$, E_g, and T_{2g}. Three independent polarization measurements fully characterize the polarization dependence of single-beam two-photon transitions of sites with O_h symmetry.[6] The multiplet to multiplet transition line strength for this symmetry simplifies to

$$I(\eta_f J_f,\eta_i J_i)=\sum_{Ja\lambda} P_\lambda \frac{|\langle \eta_f J_f||T^J_{a\lambda}||\eta_i J_i\rangle|^2}{2J+1}, \tag{29}$$

where

$$T^J_{a\lambda}=\sum_{SL} w_{SLJa\lambda} W^{S\cdot LJ}. \tag{30}$$

The polarization factors P_λ defined by Eq. (21) for the crystal orientations used by Downer *et al.*[6] are given in Table I.

The eigenvectors for states in $4f^7$ configuration can be calculated by fitting the experimental energy levels with a well-established phenomenological Hamiltonian.[27] The model-space eigenvectors required by our calculation can then be obtained by projecting the phenomenological eigenvectors into the corresponding model space. The model space for the initial states contains only $^8S_{7/2}$ multiplet and the model space eigenvectors can be determined solely by symmetry considerations. The model space for the final states contains all sextet terms and the model space eigenvectors will be a mixture of all sextet bases. We shall calculate the line strength between multiplets by neglect the J mixing caused by crystal field. We denote the free-ion model space multiplet eigenvector dominated by $^{2S+1}L_J$ as $[^{2S+1}L]_J$. Neglecting components with less than 1% contributions, the multiplets concerned are obtained by using the free-ion parameters for Eu^{2+}:CaF_2 given by Downer *et al.*[6] as follows:

$$[^SL]_J={}^SL_J \text{ for } {}^8S_{7/2} \text{ and all } {}^6I_J, \tag{31}$$

$$[^6P]_{7/2}=0.932\,{}^6P_{7/2}-0.363\,{}^6D_{7/2}, \tag{32}$$

$$[^6P]_{5/2}=0.934\,{}^6P_{5/2}-0.357\,{}^6D_{5/2}, \tag{33}$$

$$[^6P]_{3/2}=0.964\,{}^6P_{3/2}-0.268\,{}^6D_{3/2}, \tag{34}$$

$$[^6D]_{9/2}=0.983\,{}^6D_{9/2}-0.180\,{}^6F_{9/2}, \tag{35}$$

$$[^6D]_{7/2}=0.919\,{}^6D_{7/2}+0.346\,{}^6P_{7/2}-0.187\,{}^6F_{7/2}, \tag{36}$$

$$[^6D]_{5/2}=0.919\,{}^6D_{5/2}+0.359\,{}^6P_{5/2}-0.161\,{}^6F_{5/2}, \tag{37}$$

$$[^6D]_{3/2}=0.956\,{}^6D_{3/2}+0.267\,{}^6P_{3/2}-0.118\,{}^6F_{3/2}, \tag{38}$$

$$[^6D]_{1/2}=0.998\,{}^6D_{1/2}-0.063\,{}^6F_{1/2}. \tag{39}$$

Note that the eigenfunctions have been renormalized because we have omitted all multiplets other than sextets. It can be seen from the multiplet model space wave functions and the angular-momentum selection rules that only $W^{1\cdot 1}$, $W^{1\cdot 2}$, $W^{1\cdot 3}$, and $W^{1\cdot 6}$ in Eq. (13) contribute to the TPA intensities for these transitions. The expressions for the corresponding coefficients in terms of energy level parameters and the values for the case of Eu^{2+} in CaF_2 are given in Table II.

The RME's of $W^{1\cdot K}$ between sextets and octets are given by

$$\langle {}^6L||W^{1\cdot K}||{}^8S\rangle=(-1)^{K+1}\delta_{LK}2[2(2K+1)]^{1/2}, \tag{40}$$

from which we can calculate the RME's between two multiplets. The RME's used in our calculations are given in Table III.

It can be seen from the wave functions for each multiplet and the comparable magnitude of $w_{1,\cdots KJa'\lambda}$ that the intensities for final states ^6I_J $(J=7/2,\ldots,17/2)$ and ^6D_J $(J=3/2,\ldots,9/2)$ arise mainly from the contributions from $W^{1.6Ja'\lambda}$ and $W^{1.2Ja'\lambda}$ respectively and depend on $\eta=\xi_{5d}/\xi_{4f}$(normally<1) weakly. In contrast, the intensities for ^6P_J depend strongly on the ratio η. The calculated intensities for the three polarizations and the corresponding

TABLE II. The nonzero coefficients of those $W^{1KJa'\lambda}$, i. e., $w_{1\cdot KJa'\lambda}$, that contribute to the measured TPA intensities of Eu^{2+} in CaF_2. $\alpha_K^1=\alpha_K(-\epsilon_{fd}-U_d/2)$, $\alpha_K^2=\alpha_K(-\epsilon_{fd}+U_d/2)$, and $\alpha=-1/U_f$. Their values for Eu^{2+} in CaF_2 are $\alpha_0^1=-14.44/(10^5\ \mathrm{cm}^{-1})$, $\alpha_4^1=-15.76/(10^5\ \mathrm{cm}^{-1})$, $\alpha_0^2=-24.56/(10^5\ \mathrm{cm}^{-1})$, $\alpha_4^2=-41.10/(10^5\ \mathrm{cm}^{-1})$, $\alpha=-2.632/10^5\ \mathrm{cm}^{-1}$, and $\eta=\xi_{5d}/\xi_{4f}$. The unit is $\langle f|r|d\rangle^2$ for the second column and $\xi_{4f}\langle f|r|d\rangle^2/(10^5\ \mathrm{cm}^{-1})^2$ for the third column.

$1\cdot K$	J	a'	λ	expressions for site symmetry O_h	Eu^{2+}: CaF_2
$1\cdot1$	0		A_{1g}	$3\frac{\sqrt{35}}{35}\xi_{4f}(\alpha_0^1-\alpha_0^2)\alpha+\frac{\sqrt{14}}{35}\xi_{5d}(\alpha_0^1\alpha_0^2-\frac{2}{27}\alpha_4^1\alpha_4^2)$	$-11.4+32.1\eta$
$1\cdot1$	2		E_g	$-9\frac{\sqrt{35}}{350}\xi_{4f}\left[(\alpha_0^1-\alpha_0^2)+\frac{\sqrt{6}}{126}(\alpha_4^1-\alpha_4^2)\right]\alpha$	$3.59-6.99\eta$
				$-\frac{\sqrt{14}}{175}\xi_{5d}\left[\alpha_0^1\alpha_0^2+\frac{\sqrt{6}}{56}(\alpha_0^1\alpha_4^2+\alpha_4^1\alpha_0^2)-\frac{37}{378}\alpha_4^1\alpha_4^2\right]$	
$1\cdot1$	2		T_{2g}	$-9\frac{\sqrt{35}}{350}\xi_{4f}\left[(\alpha_0^1-\alpha_0^2)-\frac{\sqrt{6}}{189}(\alpha_4^1-\alpha_4^2)\right]\alpha$	$3.31-6.04\eta$
				$-\frac{\sqrt{14}}{175}\xi_{5d}\left[\alpha_0^1\alpha_0^2-\frac{\sqrt{6}}{84}(\alpha_0^1\alpha_4^2+\alpha_4^1\alpha_0^2)-\frac{11}{189}\alpha_4^1\alpha_4^2\right]$	
$1\cdot2$	2		E_g	$-3\frac{\sqrt{105}}{350}\xi_{4f}\left[(\alpha_0^1+\alpha_0^2)+\frac{\sqrt{6}}{126}(\alpha_4^1+\alpha_4^2)\right]\alpha+\frac{\sqrt{7}}{2940}\xi_{5d}(\alpha_0^1\alpha_4^2-\alpha_4^1\alpha_0^2)$	$-9.07+0.156\eta$
$1\cdot2$	2		T_{2g}	$-3\frac{\sqrt{105}}{350}\xi_{4f}\left[(\alpha_0^1+\alpha_0^2)-\frac{\sqrt{6}}{189}(\alpha_4^1+\alpha_4^2)\right]\alpha-\frac{\sqrt{7}}{4410}\xi_{5d}(\alpha_0^1\alpha_4^2-\alpha_4^1\alpha_0^2)$	$-8.67-0.104\eta$
$1\cdot2$	3		T_{2g}	$-\frac{\sqrt{14}}{8820}\xi_{5d}(\alpha_0^1\alpha_4^2-\alpha_4^1\alpha_0^2)$	-0.073η
$1\cdot3$	2		E_g	$+3\frac{\sqrt{105}}{175}\xi_{4f}\left[(\alpha_0^1-\alpha_0^2)+\frac{\sqrt{6}}{126}(\alpha_4^1-\alpha_4^2)\right]\alpha$	$-4.14+16.8\eta$
				$+3\frac{\sqrt{42}}{350}\xi_{5d}\left[\alpha_0^1\alpha_0^2+\frac{\sqrt{6}}{756}(\alpha_0^1\alpha_4^2+\alpha_4^1\alpha_0^2)-43/567\alpha_4^1\alpha_4^2\right]$	
$1\cdot3$	2		T_{2g}	$3\frac{\sqrt{105}}{175}\xi_{4f}\left[(\alpha_0^1-\alpha_0^2)-\frac{\sqrt{6}}{189}(\alpha_4^1-\alpha_4^2)\right]\alpha$	$-3.83+19.1\eta$
				$+3\frac{\sqrt{42}}{350}\xi_{5d}\left[(\alpha_0^1\alpha_0^2)-\frac{\sqrt{6}}{1134}(\alpha_0^1\alpha_4^2+\alpha_4^1\alpha_0^2)-\frac{124}{1701}\alpha_4^1\alpha_4^2\right]$	
$1\cdot3$	3		T_{2g}	$+1\frac{\sqrt{5}}{2520}\xi_{5d}[(\alpha_0^1\alpha_4^2+\alpha_4^1\alpha_0^2)-2\sqrt{6}9\alpha_4^1\alpha_4^2]$	0.538η
$1\cdot3$	4		A_{1g}	$-11\sqrt{5}630\xi_{4f}(\alpha_4^1-\alpha_4^2)\alpha-\frac{\sqrt{2}}{140}\xi_{5d}\left[(\alpha_0^1\alpha_4^2+\alpha_4^1\alpha_0^2)-2\frac{\sqrt{6}}{9}\alpha_4^1\alpha_4^2\right]$	$2.18-6.13\eta$
$1\cdot3$	4		E_g	$+\frac{\sqrt{14}}{441}\xi_{4f}(\alpha_4^1-\alpha_4^2)\alpha+\frac{\sqrt{35}}{2940}\xi_{5d}\left[(\alpha_0^1\alpha_4^2+\alpha_4^1\alpha_0^2)-2\frac{\sqrt{6}}{9}\alpha_4^1\alpha_4^2\right]$	$-0.474+1.22\eta$
$1\cdot3$	4		T_{2g}	$+\frac{\sqrt{14}}{882}\xi_{4f}(\alpha_4^1-\alpha_4^2)\alpha+\frac{\sqrt{35}}{5880}\xi_{5d}\left[(\alpha_0^1\alpha_4^2+\alpha_4^1\alpha_0^2)-2\frac{\sqrt{6}}{9}\alpha_4^1\alpha_4^2\right]$	$-0.237+0.610\eta$
$1\cdot6$	5		E_g	$+\frac{\sqrt{715}}{4620}\xi_{5d}(\alpha_0^1\alpha_4^2-\alpha_4^1\alpha_0^2)$	1.00η
$1\cdot6$	5		T_{2g}	$+\frac{\sqrt{715}}{3465}\xi_{5d}(\alpha_0^1\alpha_4^2-\alpha_4^1\alpha_0^2)$	1.33η
$1\cdot6$	6		E_g	$+\frac{\sqrt{385}}{154}\xi_{4f}\left[(\alpha_4^1+\alpha_4^2)\alpha-\frac{\sqrt{10}}{15}(\alpha_0^1\alpha_4^2-\alpha_4^1\alpha_0^2)\xi_{5d}\right]$	$18.2-4.65\eta$
$1\cdot6$	6	0	T_{2g}	$-\frac{\sqrt{2}}{21}\left[\xi_{4f}(\alpha_4^1+\alpha_4^2)\alpha-\frac{\sqrt{10}}{15}\xi_{5d}(\alpha_0^1\alpha_4^2-\alpha_4^1\alpha_0^2)\right]$	$-9.63+2.46\eta$
$1\cdot6$	2	1	T_{2g}	$-3\frac{\sqrt{110}}{308}[\xi_{4f}(\alpha_4^1+\alpha_4^2)\alpha-\sqrt{10}/15\xi_{5d}(\alpha_0^1\alpha_4^2-\alpha_4^1\alpha_0^2)]$	$-14.6+3.72\eta$

TABLE III. Reduced matrix elements for the coupled double tensors $W^{1\cdot KQ}$ between pure SL multiplets ${}^6L_J$ and ${}^8S_{7/2}$.

J	1/2	3/2	5/2	7/2	9/2	11/2
$\langle {}^6P_J \Vert W^{1.10} \Vert {}^8S_{\frac{7}{2}} \rangle$				$2\sqrt{\frac{2}{3}}$		
$\langle {}^6P_J \Vert W^{1.12} \Vert {}^8S_{\frac{7}{2}} \rangle$		$4\sqrt{\frac{1}{3}}$	$6\sqrt{\frac{1}{7}}$	$2\sqrt{\frac{5}{7}}$		
$\langle {}^6D_J \Vert W^{1.22} \Vert {}^8S_{\frac{7}{2}} \rangle$		$\frac{4}{\sqrt{21}}$	$3\sqrt{\frac{2}{7}}$	$\frac{10}{\sqrt{21}}$	$\sqrt{\frac{110}{21}}$	
$\langle {}^6D_J \Vert W^{1.23} \Vert {}^8S_{\frac{7}{2}} \rangle$	$-2\sqrt{\frac{2}{3}}$	$-4\sqrt{\frac{2}{7}}$	$-\frac{6}{\sqrt{7}}$	$-2\sqrt{\frac{22}{21}}$	$-2\sqrt{\frac{11}{21}}$	
$\langle {}^6F_J \Vert W^{1.32} \Vert {}^8S_{\frac{7}{2}} \rangle$		$\frac{2}{7\sqrt{3}}$	$\frac{2\sqrt{3}}{7}$	$\frac{4}{7}\sqrt{\frac{10}{3}}$	$\frac{10}{7}\sqrt{\frac{5}{3}}$	$2\sqrt{\frac{15}{7}}$
$\langle {}^6F_J \Vert W^{1.33} \Vert {}^8S_{\frac{7}{2}} \rangle$	$-\sqrt{\frac{2}{21}}$	$-\sqrt{\frac{5}{7}}$	$-\sqrt{\frac{15}{7}}$	$-2\sqrt{\frac{22}{21}}$	$-5\sqrt{\frac{5}{21}}$	$-\sqrt{\frac{39}{7}}$
$\langle {}^6F_J \Vert W^{1.34} \Vert {}^8S_{\frac{7}{2}} \rangle$	$3\sqrt{\frac{2}{7}}$	$\frac{15}{7}$	$\frac{5\sqrt{11}}{7}$	$\frac{2\sqrt{66}}{7}$	$\sqrt{\frac{195}{7}}$	$\sqrt{\frac{13}{7}}$
J	7/2	9/2	11/2	13/2	15/2	17/2
$\langle {}^6I_J \Vert W^{1.65} \Vert {}^8S_{\frac{7}{2}} \rangle$	$-\frac{2}{\sqrt{39}}$	$-2\sqrt{\frac{5}{39}}$	$-\frac{12}{\sqrt{91}}$	$-5\sqrt{\frac{2}{13}}$	$-10\sqrt{\frac{22}{273}}$	$-3\sqrt{\frac{22}{13}}$
$\langle {}^6I_J \Vert W^{1.66} \Vert {}^8S_{\frac{7}{2}} \rangle$	$\frac{2}{\sqrt{3}}$	$\frac{10}{7}\sqrt{\frac{5}{3}}$	$\frac{12\sqrt{2}}{7}$	$\sqrt{\frac{170}{21}}$	$\frac{2\sqrt{110}}{7}$	$\frac{3\sqrt{38}}{7}$

experimental data for multiplet to multiplet TPA intensities with $\eta = 0.60$ are plotted in Fig. 3. The calculated intensities have been scaled to match the measured intensities for ${}^6D_{9/2}$. The overall agreement between the calculated and the measured relative TPA line strengths is very good, except that for $[{}^6D]_{1/2}$, where the calculated intensities is negligible because we do not consider the "J mixing" of wave functions in our model. The most significant J mixing in $[{}^6D]_{1/2}$ will be ${}^6I_{7/2}$ and ${}^6D_{7/2}$ due to crystal-field interactions. A few percent of ${}^6I_{7/2}$ and/or ${}^6D_{7/2}$ mixed in $[{}^6D]_{1/2}$ could explain the measured intensities. The calculated intensities for $[{}^6P]_{3/2}$ are very small, and the TPA transitions have not been observed. The calculated intensities for $[{}^6P]_{7/2}$ and $[{}^6P]_{5/2}$ are greatly improved and are in good agreement with the measurements. The predictions of JPD theory for a linearly polarized transition to $[{}^6P]_{7/2}$ are larger than measurements by two orders of magnitude, and for other observable transitions to the $[{}^6P]$ multiplets and the $[{}^6D]$ multiplet are larger

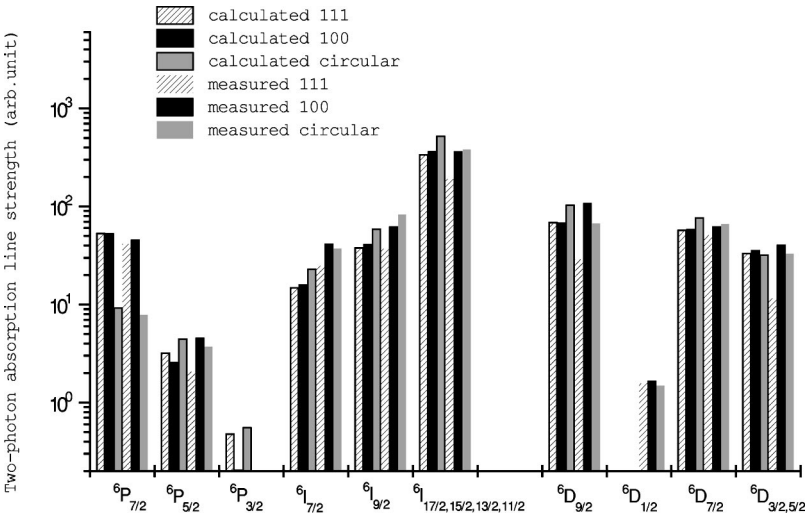

FIG. 3. Relative TPA cross sections for Eu^{2+}:CaF_2 for the three different polarizations used by Downer *et al.* (Ref. 6). For each column, the first three bars (with solid borders) are calculated and the other three bars (with dashed borders) are taken from Downer *et al.* (Ref. 6) (the measured intensities are in arbitrary units and have been scaled to match the calculated intensities for $[{}^6D]_{9/2}$). The intensities for $[{}^6P]_{3/2}$ are too small to measure, and the calculated intensities for $[{}^6D]_{1/2}$ are negligibly small, and so these results do not appear in the figure.

than measurements by one order of magnitude. For the $[^6I]$ multiplets, the agreement between our calculations and the measurements is also much better than predictions of JPD theory. Another important aspect is the polarization dependence of the TPA. For the $[^6P]_{7/2}$ multiplet, the calculated intensity for circular polarization is only one-sixth of that for the linear polarization, in good agreement with the measurements. For the $[^6I]$ multiplets and the $[^6D]$ multiplets, the absorption of the (111) beam is calculated to be only slight weaker than or equal to that of (100), and is about two-thirds of that of the circular polarization. However, the experimental intensities for (111) are significantly smaller. The relative TPA intensities change very little with a larger U_d (i.e., using the calculated value 7500 cm^{-1}) if a slightly larger $\eta = \xi_{5d}/\xi_{4f}$ (i.e., 0.65) is used.

The transition intensities for individual lines can also be calculated by using Eq. (20), provided that the wave functions for stark levels are known. However, it is well-known that for ions with a half-filled shell, the correlation crystal field is important in fitting the crystal-field energy levels, and the wave function depends strongly on the correlation crystal field[21] and the fitting of energy levels is not a easy task. Our method could also be extended to include g orbitals in intermediate states and the ligand polarization proposed by Reid and Richardson.[28]

IV. ANALYSIS OF THE TPA LINEWIDTH OF Eu^{2+}:CaF_2

For the TPA in Eu^{2+}:CaF_2,[3,5] typical linewidths for transitions to the ^6P multiplets (energy $E = 27550–28000$ cm^{-1}), the ^6I multiplets ($E = 30700–31800$ cm^{-1}), and the ^6D multiplets ($E = 33850–34950$ cm^{-1}) are approximately 2, 30, and 60 cm^{-1}, respectively. Surprisingly, there are some sharp peaks in the ^6I region and the $^6D_{1/2}$ peak, in the middle of the ^6D region, has a linewidth of approximately 8 cm^{-1}. Downer *et al.*[6] explained the general trend of the linewidths in terms of the nonradiative relaxation of $4f^7$ states to those $4f^6 5d$ states: the lowest $4f^6 5d$ states are octets and relaxation from the ^6P multiplets to these octets is spin forbidden and consequently the lines are sharp; there are some sextet $4f^6 5d$ energy levels low enough that the ^6I multiplets can relax to them, and therefore the lines are much broader; the ^6D multiplets have even more sextets available to relax to and so the lines are even broader. However the exceptions were not explained. In the following we use various selection rules to explain the linewidths.

We can write an approximate effective Hamiltonian for the $4f^6 5d$ states $(^7F,^2e)$ as follows:

$$H_{\rm eff}(^7F,^2e) = E_{\rm av} - \frac{2U_d}{7}\mathbf{S_f}\cdot\mathbf{s_d} + \frac{\xi_{4f}}{6}\mathbf{S_f}\cdot\mathbf{L_f}. \tag{41}$$

Here $E_{\rm av}$ is the barycenter energy of the $(^7F,^2e)$ states, which does not contribute to the splitting. The second term represents the exchange interaction between $4f^6$ and $5d$, which splits $(^7F,^2e)$ into an octet and a sextet. The third term represents the spin-orbit interaction of the $4f$ electrons, which is smaller in magnitude than the second term (the spin-orbit interaction of $5d$ cannot split the ^2e states, and is not included). The part of the direct Coulomb interaction that shifts $(^7F,^2e)$ as a whole can be absorbed into $E_{\rm av}$. The remaining Coulomb interaction between $4f^6$ and $5d$ and the $4f$ crystal-field interactions are neglected.

In order to solve Hamiltonian (41), we shall define two angular-momentum operators, i.e.,

$$\mathbf{S} = \mathbf{S}_f + \mathbf{S}_d, \tag{42}$$

$$\mathbf{J} = \mathbf{S} + \mathbf{L}_f. \tag{43}$$

S is the angular momentum for the total spin. **S** commutes with the second term of effective Hamiltonian (41), which gives the majority of the splitting. **J** is an angular-momentum operator that commutes with $H_{\rm eff}$. Note that **J** is different from the total angular-momentum operator of $4f^6 5d$ system in that it does not include the orbital angular momentum of the $5d$ electrons, which can be considered to be quenched by the crystal-field splitting. $\mathbf{S}^2$, $\mathbf{L_f}^2$, and **J** commute and therefore have common eigenfunctions $|^{2S+1}F_J\rangle$ ($J = 1/2,\ldots,11/2$ for $S = 5/2$ and $J = 1/2,\ldots,13/2$ for $S = 7/2$), which can be chosen as bases for $(^7F,^2e)$.

The matrix elements of the effective Hamiltonian (41) can be written as

$$\begin{aligned}\langle ^{2S+1}F_J|H_{\rm eff}(^7F,^2e)|^{2S'+1}F_{J'}\rangle &= \delta_{JJ'}\left\{\delta_{SS'}\left[\frac{U_d}{28}[51-4S(S+1)] + \xi_{4f}\left(\frac{\left(2-\frac{2S+1}{7}\right)(2J+1)^2}{48}-2\right)\right]\right. \\ &\left. - \delta_{S,S'\pm 1}\frac{\xi_{4f}}{24}(2J+1)\sqrt{1-\left(\frac{2J+1}{14}\right)^2}\right\}.\end{aligned} \tag{44}$$

Since there is only one state with $J = 13/2$, one of the the eigenvectors for the effective Hamiltonian is $^8F_{13/2}$, with an eigenvalue $E_{\rm av} - 3U_d/7 + 3\xi_{4f}/2$. The other eigenvectors and eigenvalues are obtained by diagonalizing 2×2 matrices. Since the exchange interaction is much larger than the spin-orbit interaction, the matrices are approximately diagonal and so the eigenvectors are approximately $^{2S+1}F_J$ and the corresponding eigenvalues are approximately the diagonal matrix elements $\langle ^{2S+1}F_J|H_{\rm eff}(^7F,^2e)|^{2S+1}F_J\rangle$, with only small corrections from off-diagonal matrix elements.

The vibronic crystal-field Hamiltonian responsible for nonradiative relaxation that links $4f^7$ states with $4f^6 5d$ states annihilates (creates) a $5d$ electron and creates (annihilates) an $4f$ electron. Hence it can be written in second quantized form as

$$H_{\rm int} = \sum_{k,q} b_q^k (a_f{}^{+\ (1/2\cdot 3)} a_d^{(1/2\cdot 2)})_q^{(0\cdot k)k} + \text{c.c.}, \tag{45}$$

where b_q^k ($k=1,3,5$, $q=-k,-k+1\cdots k$) are odd-parity dynamic crystal-field parameters, and the complex conjugate (c.c.) is required to make $H_{\rm int}$ hermitian. The dynamic crystal-field interaction is spin independent and of odd parity. Therefore, the spins of the creation and annihilation operators must couple to give a spin scalar ($S=0$) and the orbital angular momentum of a $4f$ electron (3) and of a $5d$ electron (2) must couple to give an odd total orbital angular momentum k. Since the orbital angular momentum of the $5d$ electron is considered to be quenched, the angular-momentum operator defined by Eq. (43) has a total spin 0 coupled with the f electron orbit angular momentum 3, and so the resulting quantum number for the operator **J** in Eq. (43) can only be 3. This is clearer if we rewrite $H_{\rm int}$ in the following form:

$$H_{\rm int}=\sum_{k,q} b_q^k (a_f^+ a_d)_q^{(((\frac{1}{2}\cdot\frac{1}{2})0\cdot 3)3\cdot 2)k}+\text{c.c.} \qquad (46)$$

Now we consider the $4f^7$ states. Neglecting the "J mixing" caused by the crystal-field interaction and the "S mixing" caused by the spin-orbit interaction, the $4f^7$ states can be written as $^{2S_f+1}L_{fJ_f}$. Since $4f^7$ contains no $5d$ electrons the quantum number for **S** in Eq. (42) is just S_f and the quantum number for **J** in Eq. (43) is just J_f.

The nonradiative relaxation of $|4f^{7\,2S_f+1}L_{fJ_f}\rangle$ to $|4f^6 5d^{2S+1}F_J\rangle$ due to $H_{\rm int}$ will therefore obey the following selection rules:

$$S_f=S, \qquad (47)$$

$$|3-J_f|\leqslant J\leqslant|3+J_f|. \qquad (48)$$

A schematic diagram of the energy levels of $4f^7$ and $4f^6 5d$ is given in Fig. 4. Note that the J label for $4f^6 5d$ is the quantum number for **J** defined by Eq. (43), rather than the usual total angular momentum. The states of $(^7F,^2e)$, characterized by quantum numbers S and J, are shifted and split by previously neglected interactions by a few hundred wave numbers. This is indicated by the shaded areas in the figure. In the figure we have used $U_d\approx 6500\ \text{cm}^{-1}$ and $\xi_{4f}=1200\ \text{cm}^{-1}$. This U_d value is necessary to have the sextet states low enough to explain the nonradiative relaxation. Now we can explain the various linewidths for the TPA spectra. The narrow linewidth of the ^6P_J states can be explained by spin selection rules because there are only octet states of $4f^6 5d$ for them to relax to. The broadening of some of the ^6I states is due to spin-allowed nonradiative relaxation of them to the sextet $4f^6 5d$ states below. The selection rule for **J** indicates that the $^6I_{J_f}$ states of $4f^7$ can only relax rapidly to ^6F_J states of $4f^6 5d$ with $J\geqslant J_f-3$. Since only states of $J\leqslant 7/2$ are close in energy to the $^6I_{J_f}$ states (see Fig. 4), the $^6I_{J_f}$ states with $J_f\geqslant 15/2$ cannot relax efficiently, so these lines are sharp. For $^6D_{J_f}$ the only nearby $4f^6 5d$ states have $J=11/2$ and 9/2 and so the $^6D_{1/2}$ state cannot relax efficiently, giving a sharp line. Note that even the "sharp" ^6I and ^6D lines are broader than the ^6P lines, due to the "J-mixing" breaking down the selection rules.

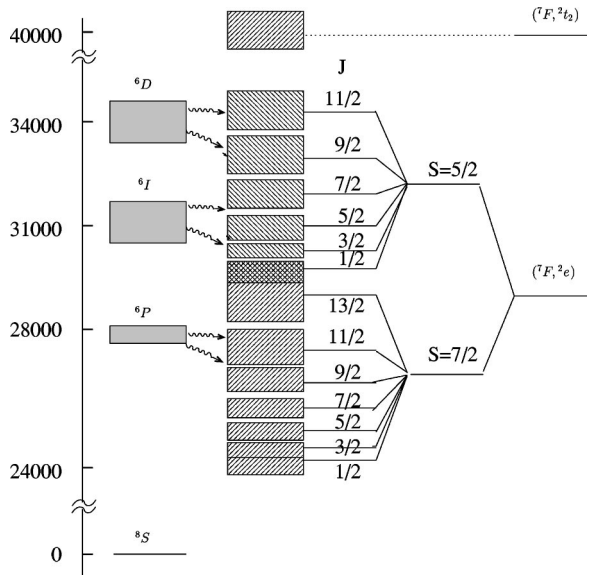

FIG. 4. Schematic diagram of the energy levels of $4f^7$ and $4f^6 5d$. Note that the J label for $4f^6 5d$ is the quantum number for the **J** defined by Eq. (43), rather than the usual total angular momentum. The states of $(^7F,^2e)$, characterized by quantum number S and J are further shifted and split by a few hundred wave numbers by interactions not included in the Hamiltonian [Eq. (41)]. This is indicated by the shaded areas in the figure. In the figure we have used $U_d\approx 6500\ \text{cm}^{-1}$ and $\xi_{4f}=1200\ \text{cm}^{-1}$.

V. CONCLUSION

A simple method to calculate the spin-forbidden two-photon transition rates for f^N ($N=6$, 7, and 8) ions in crystals based on many-body perturbation theory and group theory has been developed. This theory includes the excited-state crystal-field interactions and the dominant part of Coulomb splitting in the zeroth-order Hamiltonian. A particular case of this method, the TPA of a f^N ion in an O_h site, is treated in detail, and a comparison with experimental data is made for Eu^{2+} ($4f^7$) in CaF_2. The theory reproduces the measurements very well. The dependence of two-photon transition intensities on the spin-orbit interaction parameters is made clear with this method. This solves the so-called "unusual weakness of third-order spin-orbit contributions."[6] This method could be extended to include other intermediate states and ligand polarizations. It is expected that the method herein can also solve the puzzling problems of the spin and orbit-forbidden two-photon transitions in other cases such as Sm^{2+} in SrF_2 and Eu^{2+} in $KMgF_3$.[14]

Nonradiative relaxation mechanisms have also been considered. The unusually small linewidths for some TPA peaks have been explained by angular-momentum selection rules for nonradiative relaxation based on a simple effective Hamiltonian.

*Permanent address: Department of Mathematics and Physics, Chongqing University of Post and Telecommunication, Chongqing, 400065, Peoples Republic of China.

[1] M. C. Downer, in *Laser Spectroscopy of Solids II*, edited by W. M. Yen (Springer-Verlag, Berlin, 1989), Chap. 2.

[2] M. Dagenais, M. Downer, R. Neumann, and N. Bloembergen, Phys. Rev. Lett. **46**, 561 (1981).

[3] M. C. Downer, A. Bivas, and N. Bloembergen, Opt. Commun. **41**, 335 (1982).

[4] M. C. Downer and A. Bivas, Phys. Rev. B **28**, 3677 (1983).

[5] M. C. Downer, Ph.D thesis, Harvard University, Cambridge, MA, 1983.

[6] M. C. Downer, C. D. Cordero-Montalvo, and H. Crosswhite, Phys. Rev. B **28**, 4931 (1983).

[7] J. D. Axe, Phys. Rev. **136**, A42 (1964).

[8] L. Smentek, Phys. Rep. **297**, 156 (1998).

[9] B. R. Judd and D. R. Pooler, J. Phys. C **15**, 591 (1982).

[10] A. Ceulemans and G. M. Vandenberghe, J. Chem. Phys. **98**, 9372 (1993); **102**, 7762(E) (1995).

[11] A. Ceulemans and G. M. Vandenberghe, Phys. Rev. B **53**, 8310 (1996).

[12] J. C. Gâcon, G. W. Burdick, and B. Moine, Phys. Rev. B **47**, 11 712 (1993).

[13] M. Chua and P. A. Tanner, Phys. Rev. B **56**, 7967 (1997).

[14] R. Francini, U. M. Grassano, S. Boiko, G. G. Tarasov, and A. Scacco, J. Chem. Phys. **110**, 457 (1999).

[15] K. M. Murdoch, A.-D. Nguyen, and N. M. Edelstein, Phys. Rev. B **56**, 3038 (1997).

[16] K. M. Murdoch, A.-D. Nguyen, and N. M. Edelstein, J. Lumin. **79**, 55 (1998).

[17] G. W. Burdick and M. F. Reid, Phys. Rev. Lett. **70**, 2491 (1993); **71**, 3892 (1993).

[18] M. F. Reid, G. W. Burdick, and H. J. Kooy, J. Alloys Compd. **207/208**, 78 (1994).

[19] G. W. Burdick, H. J. Kooy, and M. F. Reid, J. Phys.: Condens. Matter **5**, L323 (1993).

[20] L. van Pieterson, M. F. Reid, G. W. Burdick, and A. Meijerink, Phys. Rev. B **65**, 045114 (2002).

[21] G. W. Burdick, A. Burdick, C. K. Duan, and M. F. Reid (unpublished).

[22] Special care needs to be taken in treating the Coulomb interaction as a perturbation in JPD theory. The initial and final states for TPA are exact eigenvectors in a basis that includes the whole f^N configuration. Since they are not eigenstates of the total spin, the contribution of first order in the Coulomb interaction but zeroth order in the spin-orbit interaction should be taken into account. These have generally been neglected. This contribution could be important since the Coulomb interaction is much stronger than the spin-orbit interactions.

[23] P. H. Butler, *Point Group Symmetry Applications: Methods and Tables* (Plenum Press, New York, 1981).

[24] H. J. Ross, L. F. McAven, K. Shinagawa, and P. H. Butler, J. Comput. Phys. **128**, 331 (1996).

[25] C. W. Nielson, G. F. Koster, *Spectroscopic Coefficients for the p^n, d^n and f^n Configurations* (MIT Press, Cambridge, MA, 1963).

[26] R. D. Cowan, *The Theory of Atomic Structure and Spectra* (University of California Press, Berkeley, 1981).

[27] W. T. Carnall, G. L. Goodman, K. Rajnak, and R. S. Rana, J. Chem. Phys. **90**, 3443 (1989).

[28] M. F. Reid and F. S. Richardson, Phys. Rev. B **29**, 2830 (1984).